THE JOURNAL OF PHYSICAL CHEMISTRY A
A JOURNAL OF THE AMERICAN CHEMICAL SOCIETY

pubs.acs.org/JPCA

Article

Charge-Separation and Charge-Recombination Rate Constants in a Donor–Acceptor Buckybowl-Based Supramolecular Complex: Multistate and Solvent Effects

Jesús Cerdá, Joaquín Calbo, Enrique Ortí, and Juan Aragó*

Cite This: *J. Phys. Chem. A* 2021, 125, 9982–9994

Read Online

ACCESS | Metrics & More | Article Recommendations | Supporting Information

ABSTRACT: The kinetics of the nonradiative photoinduced processes (charge-separation and charge-recombination) experimented in solution by a supramolecular complex formed by an electron-donating bowl-shaped truxene-tetrathiafulvalene (truxTTF) derivative and an electron-accepting fullerene fragment (hemifullerene, $C_{30}H_{12}$) has been theoretically investigated. The truxTTF·$C_{30}H_{12}$ heterodimer shows a complex decay mechanism after photoexcitation with the participation of several low-lying excited states of different nature (local and charge-transfer excitations) all close in energy. In this scenario, the absolute rate constants for all of the plausible charge-separation (CS) and charge-recombination (CR) channels have been successfully estimated using the Marcus–Levich–Jortner (MLJ) rate expression, electronic structure calculations, and a multistate diabatization method. The outcomes suggest that for a reasonable estimate of the CS and CR rate constants, it is necessary to include the following: (i) optimally tuned long-range (LC) corrected density functionals, to predict a correct energy ordering of the low-lying excited states; (ii) multistate effects, to account for the electronic couplings; and (iii) environmental solvent effects, to provide a proper stabilization of the charge-transfer excited states and accurate external reorganization energies. The predicted rate constants have been incorporated in a simple but insightful kinetic model that allows estimating global CS and CR rate constants in line with the most generalized three-state model used for the CS and CR processes. The values computed for the global CS and CR rates of the donor–acceptor truxTTF·$C_{30}H_{12}$ supramolecular complex are found to be in good agreement with the experimental values.

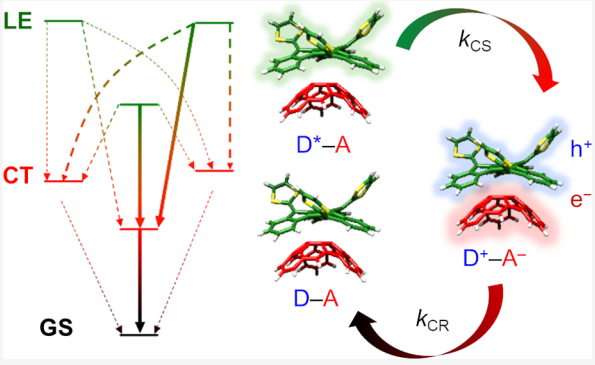

INTRODUCTION

Since their discovery,[1,2] organic solar cells (OSCs) have been considered as potential alternatives to silicon photovoltaic cells, mainly due to their low cost, easy processing, and low toxicity.[3] Although there has been no improvement in the performance of OSCs for many years, recent breakthroughs pushing the performance above 17% have again reawakened the interest in this photovoltaic technology.[4,5] OSCs are usually made of an active layer formed by a mixture of organic semiconducting molecules with donor and acceptor characteristics (bulk heterojunction), which is sandwiched between two electrodes. In general, the processes occurring in a standard OSC can be summarized as follows: (i) light absorption by the donor compound (exciton formation), (ii) exciton migration to the interface between the donor and acceptor, and (iii) electron transfer from the donor to the acceptor (*i.e.*, charge separation, CS), with the consequent generation of a charge-transfer (CT) state. At this point, two possible paths can take place, either (iv) the detrimental process by which the separated charges recombine coming back to the ground state (*i.e.*, charge recombination, CR) or (v) the generated charges overcome the Coulombic attraction and migrate to the respective electrodes giving rise to the desired photocurrent.

If we turn our attention to the active materials involved in OSCs, fullerenes and fullerene derivatives are the most used electron-acceptor systems for OSC applications.[6−9] In particular, [6,6]-phenyl-C_{61}-butyric acid methyl ester (known as PCBM) is likely to be the most employed acceptor for bulk heterojunction solar cells.[10−12] The combination of PCBM with poly(3-hexylthiophene) (P3HT), acting as a donor, has been widely studied as a model system to gain insight into the elementary physical processes occurring in OSCs.[3,13−15] In the last years, the quest for novel non-fullerene acceptors for photovoltaic applications has emerged as an active research field to boost the potential and application of OSCs.[16−19] Recently, novel fullerene fragments known as buckybowls (*e.g.*,

Received: June 29, 2021
Revised: October 27, 2021
Published: November 12, 2021

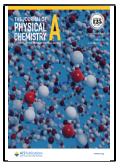

https://doi.org/10.1021/acs.jpca.1c05740
J. Phys. Chem. A 2021, 125, 9982–9994

$C_{30}H_{12}$, $C_{32}H_{12}$, and $C_{38}H_{14}$) have been synthesized (Figure 1).[20−22] These buckybowls mimic the electron-acceptor

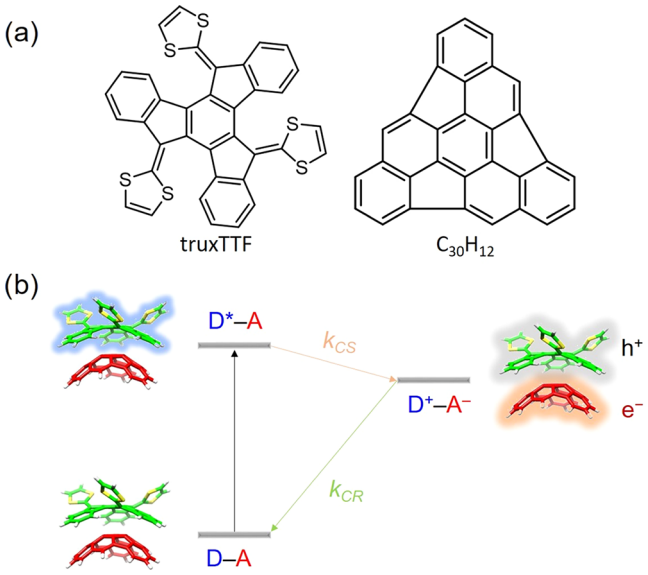

Figure 1. (a) Chemical structures of the donor truxTFF and the acceptor buckybowl $C_{30}H_{12}$ (hemifullerene). (b) Schematic representation of the charge-separation and charge-recombination photophysical processes taking place in the donor−acceptor supramolecular truxTTF·$C_{30}H_{12}$ complex.

behavior of C_{60} when combined supramolecularly with the truxene-tetrathiafulvalene (truxTTF) electron-donor derivative (Figure 1), exhibiting an efficient photoinduced CS process and a slower CR event, and may therefore be considered as potential candidates in the context of OSCs.[23,24]

From a computational perspective, the usual approximations to evaluate the CS and CR rate constants rely on the use of the classical Marcus equation or the semiclassical Marcus−Levich−Jortner (MLJ) variant.[25,26] The use of these two rate expressions requires the accurate estimation of the energies of the initial and final electronic states involved in the electron-transfer process. Time-dependent density functional theory (TDDFT) is likely to be the electronic structure method most widely used to theoretically estimate the energy position of the excited states implied in photoinduced electron-transfer events at a molecular scale. Nevertheless, TDDFT, when combined with standard GGA and hybrid density functionals, holds inherent drawbacks concerning the energy prediction of CT excited states (usually a significant underestimation) due to self-interaction errors.[27−29] Long-range corrected (LC) density functionals (*e.g.*, LC-ωPBE,[27] CAM-B3LYP,[30] or ωB97X-D,[31] just to mention a few) were specially designed to mitigate this general drawback and other weaknesses. Although standard LC density functionals can be generally employed for different chemical applications,[32] optimally tuned LC density functionals have been demonstrated to behave more accurately for electron-transfer problems in donor−acceptor molecular heterojunctions.[33−37] In particular, optimally tuned LC density functionals are able to provide a balanced description of both local and CT excitations due to the system-dependent tuning based on physical grounds.

Solvent effects play an essential role in stabilizing the CT states and, therefore, in determining the relative energy of the excited states when the electron-transfer reaction occurs in solution. The electron-transfer rate expressions indeed require the estimation of the Gibbs free energy difference between fully relaxed states, which, in addition to geometric relaxation, implies solvent polarization and relaxation. In this context, the widely employed polarization continuum model (PCM)[38] in its standard linear-response TDDFT formalism cannot be totally adequate to capture the stabilization of the excited CT states since the solvent response acts only on the transition densities of the targeted CT states. An alternative state-specific PCM formulation,[39] where solvent−solute interactions are evaluated through the specific density of the excited states of interest, has been successfully developed to accurately capture solvent effects for spectroscopic purposes (simulation of the emission spectra and Stokes shifts).[40] Nonetheless, this state-specific PCM method has been barely employed in charge-transfer contexts.[41] In addition to continuum models, polarizable force fields explicitly including solvent molecules surrounding the supramolecular complexes have been employed to describe CT excited states in solution.[42]

Another critical aspect in the evaluation of nonadiabatic photoinduced electron-transfer rates is the estimation of the electronic couplings between the excited states involved in the electron-transfer processes.[43] Electronic couplings are usually computed using either the orbital interaction model[44,45] or two-state diabatization schemes (*e.g.*, the generalized Mulliken−Hush[46] or the fragment charge difference (FCD)[47] treatments). Both approaches present drawbacks; the former fails when more than a single monoexcitation is needed for the correct excited state description, whereas the latter may provide wrong electronic-coupling values when several excited states close in energy (*i.e.*, multistate effects) are involved in the electron-transfer processes. The relevance of multistate effects on the electronic couplings was already discussed by Cave et al.[48] in small-size molecular pairs but, surprisingly, has been hardly discussed in the context of OSCs for donor−acceptor heterojunction models. Recently, Kastinen et al.[49] have stressed its importance for poly(thiophene-*co*-quinoxaline)−$PC_{71}BM$ interfaces.

In the present work, we propose a theoretical protocol to accurately estimate the charge-separation and charge-recombination rates in donor−acceptor (D−A) supramolecular assemblies in solution. As a model system, we have selected a D−A supramolecular heterodimer formed by the electron-donor truxTTF and the hemifullerene $C_{30}H_{12}$ as the electron acceptor (Figure 1). The theoretical approximation here presented combines the Marcus−Levich−Jortner rate expression[50−52] and DFT electronic structure calculations, along with TDDFT excited-state energy levels, to carefully evaluate the different terms entering the rate expression, *i.e.*, Gibbs free energy differences, electronic couplings, and reorganization energies. For D−A supramolecular complexes involving fullerene fragments (in particular truxTTF·$C_{30}H_{12}$), and by extension fullerenes, a complex scenario with a set of low-lying, close-in-energy excited states of local and CT character is generally found, opening the door to multiple CS and CR pathways. We demonstrate that in this situation, the inclusion of multistate effects in the selected diabatization scheme is mandatory to predict reasonable electronic couplings for the different electron-transfer channels. We also highlight the relevance of the theoretical solvent model to adequately capture the energy stabilization of the CT excited states due to solvent effects (polarization and reorganization).

https://doi.org/10.1021/acs.jpca.1c05740
J. Phys. Chem. A 2021, 125, 9982−9994

METHODOLOGY

Rate Constant Expression. Assuming a weak electronic-coupling regime, the photoinduced electron-transfer events in buckybowl-based donor−acceptor supramolecular complexes can be described within a hopping mechanism by a nonadiabatic electron-transfer rate expression. Among the different electron-transfer rate expressions, the Marcus−Levich−Jortner equation was selected because it is able to incorporate quantum tunneling effects. Note that in π-conjugated semiconducting compounds, high-frequency vibrations (associated with single and double carbon−carbon stretching motions) significantly couple to the electronic states responsible for the electron-transfer processes. In contrast to the classical Marcus theory, the MLJ rate expression is able to capture quantum effects that come from the high-frequency vibrations through an effective vibrational normal mode coordinate.[50−54] The MLJ nonadiabatic electron-transfer rate is expressed as follows

$$k_{ij} = \frac{4\pi}{h}|V_{ij}|^2 \frac{1}{\sqrt{4\pi\lambda_c k_B T}} \sum_n P_T(n) \sum_m |FCI_{nm}(S_{eff})|^2 \exp\left[-\frac{(\Delta G_{ij} + \lambda_c + (m-n)h\nu_{eff})^2}{4\lambda_c k_B T}\right] \quad (1)$$

where V_{ij} is the electronic coupling between the initial i and final j electronic states, k_B is the Boltzmann constant, T is the temperature, h is the Planck constant, and ΔG_{ij} is the Gibbs free energy difference between the initial and final states. λ_c corresponds to the classical reorganization energy including intramolecular and external (solvent) components (*vide infra*). FCI_{nm} (S_{eff}) denotes the Franck−Condon integral between the initial (n) and final (m) vibrational levels of the initial i and final j electronic states, which are calculated using an analytic expression under the harmonic approximation (see eq S1 in the Supporting Information).[55] The Franck−Condon integral depends on the Huang−Rhys (HR) factor S_{eff}, which describes the relative displacement along an effective quantum normal mode with frequency ν_{eff}. Finally, $P_T(n)$ represents the Boltzmann probability that a vibrational state n on an initial electronic state i is occupied at a certain temperature. It should be noted that the rate constant in its current form is only valid for electron-transfer events within the limiting incoherent regime, where the involved electronic states in the diabatic picture are localized at molecular units. For delocalized situations, a more general rate expression would be necessary (see ref 56).

Electronic Couplings. In a system with N adiabatic (AD) electronic states $\{\psi_1, \psi_2, ..., \psi_N\}$ with energies $\{E_1, E_2, ..., E_N\}$, the adiabatic Hamiltonian matrix is diagonal ($\mathbf{H}^{AD}$). These AD states can be related to a set of N diabatic (DI) states $\{\varphi_1, \varphi_2, ..., \varphi_N\}$ by means of an orthogonal transformation as follows

$$\varphi_i = \sum_j C_{ij}\psi_j \quad (2)$$

Once the adiabatic-to-diabatic orthogonal transformation matrix $\mathbf{C}$ is determined, the diabatic and adiabatic Hamiltonians are easily connected by $\mathbf{H}^{DI} = \mathbf{C}\mathbf{H}^{AD}\mathbf{C}^T$ (diabatization), where the diagonal elements of $\mathbf{H}^{DI}$ correspond to the diabatic energies and the off-diagonal elements to the electronic couplings (V_{ij}). Although there is no unique adiabatic-to-diabatic transformation,[57] most diabatization schemes, particularly in the context of charge/energy transfer, aim to find the best unitary transformation matrix $\mathbf{C}$ that generates the closest diabatic states with respect to a set of reference states with a well-defined molecular property. Among the most popular diabatization schemes for charge transfer, the generalized Mulliken−Hush method, which employs (transition) dipole moments,[46] and the fragment charge difference (FCD) scheme,[47] which uses a charge difference operator, have to be emphasized. In this study, the FCD diabatization scheme within its multistate extension[58] was selected (see the Supporting Information for a brief description of the FCD method). We anticipate that the inclusion of multistate effects is crucial for accurate electronic-coupling predictions in D−A truxTTF·$C_{30}H_{12}$ owing to the presence of a number of low-lying singlet excited states in a narrow energy range.

Singlet Excited States and Gibbs Free Energy Difference. To describe appropriately the CS and CR processes in the D−A interface at the molecular level, it is necessary to characterize the lowest-energy singlet excited states of the supramolecular heterodimer model (in our case, truxTTF·$C_{30}H_{12}$). Triplet excited states are not considered in this work, although they may also play an active role in the photoinduced electron-transfer events in bulk heterojunctions.[59−62] The low-lying singlet excited states of the truxTTF·$C_{30}H_{12}$ complex were computed within the TDDFT approach in its Tamm−Dancoff (TDA−DFT) variant. The lowest-energy excited states in the D−A truxTTF·$C_{30}H_{12}$ heterodimer were expected to be relatively close in energy and show different nature (*i.e.*, local excitations (LE) centered in the donor/acceptor fragments or charge-transfer (CT) excitations). It is well-known that the energy estimation of CT excited states is a challenging task for TDDFT with GGA and hybrid density functionals due to self-interaction errors.[27−29,63] In contrast, long-range corrected (LC) density functionals have been demonstrated to provide a satisfactory description of CT-like excited states,[63,64] especially when these LC functionals have been optimally tuned (OT) for the specific system under study.[36,63,65−67] The tuning procedure used here was carried out in the gas phase according to eq S4[37,65,67] and was performed for both the isolated compounds (truxTTF and $C_{30}H_{12}$) and the supramolecular truxTTF·$C_{30}H_{12}$ assembly (see the Supporting Information for further details).

The adiabatic Gibbs free energy difference for CS and CR processes was computed as follows

$$\Delta G_{CS} = E_{CT} - E_{LE} \quad (3)$$

$$\Delta G_{CR} = E_{GS} - E_{CT} \quad (4)$$

Assuming that the entropic component is negligible, $\Delta G_{CS/CR}$ can be approximated as the electronic energy difference (ΔE) between the involved states at their respective minimum-energy geometry. E_{CT} denotes the energy of a D^+−A^- CT-like excited state (truxTTF$^+$·$C_{30}H_{12}^-$), whereas E_{LE} corresponds to the energy of a local-type excited state where the excitation is mainly localized on the donor (*i.e.*, truxTTF*·$C_{30}H_{12}$). E_{GS} denotes the ground-state energy of the truxTTF·$C_{30}H_{12}$ heterodimer.

Reorganization Energy. The reorganization energy (λ) is a key parameter for the evaluation of electron-transfer rates and is associated with the energy change owing to electronic redistribution and nuclear rearrangement in the electron-transfer events.[68] Generally, λ is split into internal and external reorganization components ($\lambda = \lambda_{int} + \lambda_{ext}$). The former

https://doi.org/10.1021/acs.jpca.1c05740
J. Phys. Chem. A 2021, 125, 9982−9994

accounts for the energy cost of the intramolecular nuclear relaxation of the donor and acceptor systems associated with the electron-transfer reaction. The latter comes from the environmental effects resulting from the polarization and reorientation of neighboring molecules as a response to the charge (electron or hole) injection in the donor−acceptor system.

The internal reorganization energies for the CS and CR processes (λ_{int}^{CS} and λ_{int}^{CR}) are expected to be different. For the electron-transfer D*−A → D$^+$−A$^-$ reaction (CS), λ_{int}^{CS} corresponds to the energy difference between the initial geometry (D*−A) and the final geometry (D$^+$−A$^-$) in the potential energy surface of the CT D$^+$−A$^-$ excited state. For the CR process (D$^+$−A$^-$ → D−A), λ_{int}^{CR} is estimated as the energy change between the initial geometry (D$^+$−A$^-$) and the final geometry (D−A) in the ground-state potential energy surface. Internal reorganization energies can be decomposed into contributions for each vibrational normal mode according to $\lambda_{int}^{CS/CR} = \sum_k h\nu_k S_k$,[52] where ν_k is the vibrational frequency of the normal mode k and S_k denotes the corresponding HR factor.[69] The electron-transfer reaction can be drastically but successfully simplified[70−72] to a single effective normal mode coordinate with frequency $\nu_{eff} = \sum_k \nu_k S_k / \sum_k S_k$ and an effective HR factor $S_{eff} = \lambda_{int}^{CS/CR}/h\nu_{eff}$.[44]

Concerning the external reorganization energy, there are several methods to estimate λ_{ext} in solution with different degrees of accuracy. Among them, the Marcus two-sphere model,[73] the "nonequilibrium versus equilibrium solvation" approximation,[39] and the dynamic polarization response method should be stressed.[74] Note that the calculation of λ_{ext} in solution is always associated with a significant uncertainty, and possibly, it is the parameter subject to a larger error in the electron-transfer rate expressions. In molecular crystals, λ_{ext} can be successfully evaluated based on hybrid techniques combining electronic structure calculations and polarizable force fields.[75] Nevertheless, λ_{ext} is generally small compared to λ_{int} and, therefore, less determining for the charge-transfer rates in molecular crystals. In the present work, the "nonequilibrium versus equilibrium solvation" approximation within the state-specific polarizable continuum model (SS-PCM)[39] is employed. The SS-PCM method has been already proved to satisfactorily estimate the inhomogeneous broadening of electronic transitions in solution[76] and to capture solvent effects in electron-transfer reactions.[41] Briefly, the method allows using an initial solvent configuration (nonequilibrium), where only fast polarization effects are captured, and a final solvent configuration (equilibrium), where the slow solvent reorientation has occurred. The difference between these two situations ($E_{Eq} - E_{NonEq}$) gives an estimate of the total λ ($\lambda = \lambda_{int} + \lambda_{ext}$).

Computational Details. All of the calculations were performed using the Gaussian16 package in its revision A03,[77] except for the ground-state geometries of the truxTTF·$C_{30}H_{12}$ supramolecular complex, which were extracted from previously published results at the revPBE0-D3/cc-pVTZ level.[23] Singlet excited-state calculations were performed within the TDDFT approach in its TDA−DFT variant[78] using different density functionals in combination with the Pople's 6-31G** basis set.[79] The GGA BLYP[80,81] and hybrid B3LYP[80,81] functionals, as well as the long-range corrected density functionals LC-BLYP,[64] CAM-B3LYP,[30] LC-ωPBE,[27] and ωB97X-D[82] according to the Hirao's correction,[64] were employed. Likewise, the optimally tuned versions of LC-BLYP, LC-ωPBE, and ωB97X-D (hereafter named OT-LC-BLYP, OT-LC-ωPBE, and OT-ωB97X-D, respectively) were also used. Solvent effects were taken into account within the polarizable continuum model (PCM)[74,83] with o-dichlorobenzene as the solvent. In the case of CT excited states, their energies were recalculated by performing single-point calculations using the SS-PCM approach[39] and the linear-response PCM-optimized geometries, to properly account for the CT stabilization due to environmental polarization and reorganization effects.

Electronic couplings V_{ij} were estimated using the standard two-state FCD diabatization scheme[43] and a multistate extension[58] implemented in a home-made program. The program makes use of the overlap matrix between the atomic basis functions, the molecular orbital coefficients, and the excitation coefficients obtained from TDA−DFT calculations.

RESULTS AND DISCUSSION

Supramolecular Heterodimer Structures. Four different minimum-energy structures of the supramolecular truxTTF·$C_{30}H_{12}$ heterodimer were previously reported, as shown in Figure 2.[23] The structures were calculated at the

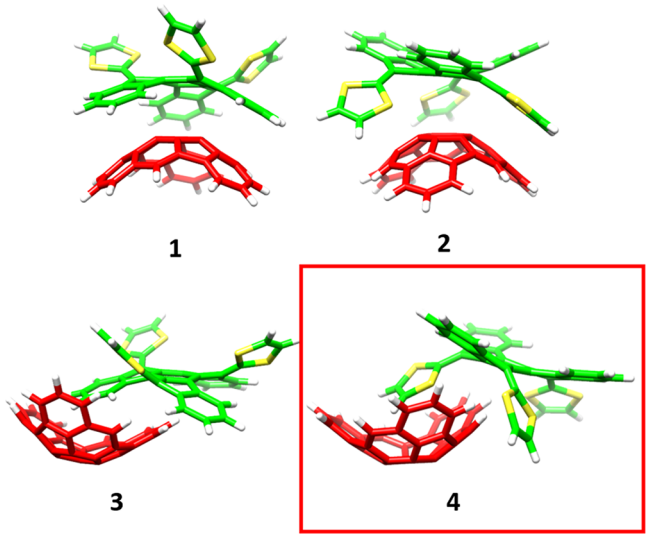

Figure 2. Minimum-energy structures computed at the revPBE0-D3/cc-pVTZ level of theory[23] for the truxTTF·$C_{30}H_{12}$ supramolecular donor−acceptor heterodimer.[23] For truxTTF: carbon atoms in green, sulfur in yellow, and hydrogen in white. For $C_{30}H_{12}$: carbon in red and hydrogen in white. The most stable structure **4** (mainly used during the discussion) is highlighted with a red square.

revPBE0-D3/cc-pVTZ level and exhibited close intermolecular contacts in the 2.5−4.0 Å range, indicative of favorable noncovalent interactions between the electron-donor truxTTF and the electron-acceptor $C_{30}H_{12}$ bowl. In structures **1** and **2** (bowl-in-bowl structures), the convex surface of the $C_{30}H_{12}$ bowl matches the two concave cavities of the truxTTF bowl; in structure **1**, the $C_{30}H_{12}$ bowl interacts with the carbon backbone of truxTTF, whereas in structure **2**, the bowl faces the cavity formed by the central benzene and the three dithiole rings. In structures **3** and **4** (staggered structures), the truxTTF is placed inside the $C_{30}H_{12}$ cavity; in structure **3**, a benzene ring is in the cavity, whereas in structure **4**, a dithiol ring is inside of $C_{30}H_{12}$. Staggered structures were predicted to be more stable than the bowl-in-bowl conformers due to the larger number of CH−π and π−π interactions that take place

https://doi.org/10.1021/acs.jpca.1c05740
J. Phys. Chem. A 2021, 125, 9982−9994

in the former. In particular, interaction energies of −25.3 and −28.1 kcal mol^{-1} were computed for structures **3** and **4**, respectively, compared with the values of −21.0 and −19.4 kcal mol^{-1} obtained for structures **1** and **2**, respectively.[23] From now on, we will keep our discussion focused on the most stable structure **4**, as this staggered structure is likely to be the most abundant in solution.[24] Nonetheless, analysis of the CS and CR rate constants and relevant parameters calculated for structures **1**−**3** are given in the Supporting Information.

Analysis of the Low-Lying Singlet Excited States. Prior to calculating ΔG_{CS} and ΔG_{CR}, which requires excited-state geometry optimizations, it is desirable to perform an analysis of the excited-state distribution at the ground-state geometry (Franck−Condon region) of truxTTF·$C_{30}H_{12}$ (structure **4**). Density functionals of different nature—GGA (BLYP), hybrid (B3LYP), and CAM-B3LYP, together with the optimally tuned long-range corrected functionals OT-LC-BLYP, OT-LC-ωPBE, and OT-ωB97X-D—were initially evaluated within the TDA−DFT approximation (6-31G** basis set in *o*-dichlorobenzene), to investigate and assess their performance. Among the analyzed density functionals, the OT-LC-BLYP(ω = 0.16 bohr^{-1}) functional showed the best performance and, therefore, was adopted for the calculation of the parameters related to the estimation of the CS and CR rate constants (see Section S2 in the Supporting Information for full details).

Figure 3a displays the vertical excitation energies, the oscillator strengths (f), and the values of the charge difference

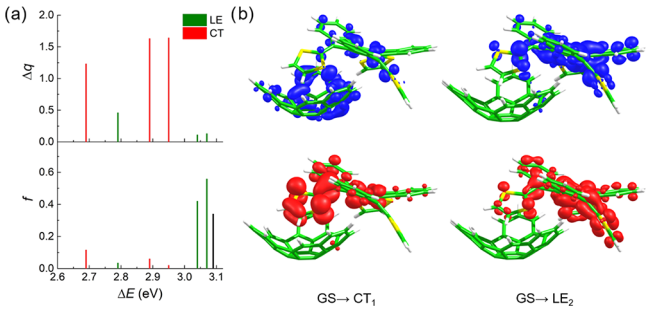

Figure 3. (a) Representation of Δq (top) and oscillator strength (f, bottom) as a function of the excitation energy (ΔE) calculated for the truxTTF·$C_{30}H_{12}$ heterodimer at the OT-LC-BLYP(ω = 0.16 bohr^{-1})/6-31G** level in *o*-dichlorobenzene within the PCM approach. The bright lowest-energy excited states (S_2 and S_3) computed for truxTTF at 3.09 eV (bottom, black bar) at the same level of theory are also indicated for comparison purposes. (b) Attachment (top) and detachment (bottom) densities computed for the lowest-energy $S_0 \rightarrow S_1$ transition of CT nature (GS → CT_1) and the bright $S_0 \rightarrow S_5$ transition with LE character (GS → LE_2).

between the donor and the acceptor (Δq) calculated for the six lowest-energy singlet excited states of the truxTTF·$C_{30}H_{12}$ assembly at the OT-LC-BLYP(ω = 0.16 bohr^{-1})/6-31G** level in the presence of *o*-dichlorobenzene within the PCM approach (see also Table S8). Vertical excitation energies and oscillator strengths for the isolated truxTTF donor are also included for comparison purposes. Δq is used as a descriptor that measures the CT character of a particular excited state (see Section S1.2 in the Supporting Information). States with Δq values above 1e indicate a significant CT character, whereas states with Δq < 0.5e are characteristic of LE excitations involving only the truxTTF donor. Values of Δq between 0.5 and 1e correspond to states with a mixed LE&CT character. All of the electronic transitions relevant for the CS and CR processes in truxTTF·$C_{30}H_{12}$ are found to be in the 2.69−3.10 eV energy window and can be classified as LE or CT excitations according to the Δq descriptor[84] and the attachment/detachment densities (Figure 3b and Table S8). The three lowest-energy CT electronic transitions ($S_0 \rightarrow S_1$, $S_0 \rightarrow S_3$, and $S_0 \rightarrow S_4$, from now on labeled as GS → CT_1, GS → CT_2, and GS → CT_3) are calculated at 2.69, 2.88, and 2.95 eV, respectively, and are mainly described by monoexcitations from the highest occupied molecular orbital (HOMO) of truxTTF to the lowest unoccupied molecular orbitals (LUMOs, LUMO + 1, and LUMO + 2, respectively) of $C_{30}H_{12}$ (Figure S3), thus implying a significant charge transfer from the donor to the acceptor. The CT character of these transitions is corroborated by the Δq descriptor with values of 1.23, 1.63, and 1.64e for CT_1, CT_2, and CT_3, respectively (Figure 3a and Table S8), and visualized by the attachment/detachment densities calculated for the GS → CT_1 (Figure 3b) and GS → CT_2, CT_3 transitions (Figure S4).

The $S_0 \rightarrow S_2$, $S_0 \rightarrow S_5$, and $S_0 \rightarrow S_6$ electronic transitions are computed at 2.79, 3.04, and 3.07 eV, respectively, and present small Δq values (0.46, 0.11, and 0.13, respectively), indicative of their LE character, as supported by the attachment/detachment densities calculated for the $S_0 \rightarrow S_5$ (Figure 3b). These transitions are hereafter named GS → LE_1, GS → LE_2, and GS → LE_3, respectively. While the GS → LE_1 transition exhibits a small oscillator strength (f = 0.035), the GS → LE_2 and GS → LE_3 excitations correspond to bright transitions with f values of 0.420 and 0.558, respectively, in line with the electronic transitions calculated for isolated truxTTF (Table S11).

The above outcomes, with the presence of at least six singlet excited states close in energy in less than 0.4 eV at the Franck−Condon region, clearly highlight a complex scenario where several charge-transfer channels can occur during the CS and CR electronic events.

Electronic Couplings. All of the electronic couplings (V_{ij}) between the low-lying LE (LE_1, LE_2, and LE_3) and CT (CT_1, CT_2, and CT_3) excited states and also the ground state for the truxTTF·$C_{30}H_{12}$ heterodimer were evaluated within the TDA−DFT approximation at the OT-LC-BLYP(ω = 0.16 bohr^{-1})/6−31G** + PCM (*o*-dichlorobenzene) level using the ground-state geometry and the FCD diabatization scheme[47] in its two-state and multistate variants (Table 1). The V_{ij} couplings estimated using the multistate FCD method are found in the 4−44 meV range and are comparable to the values reported in the literature for different D−A supramolecular heterojunc-

Table 1. Absolute Electronic Couplings V_{ij} between the Ground State (GS) and Charge-Transfer (CT) Excited States and between Local (LE) and CT Excited States Calculated Using the FCD Diabatization Scheme in Its Multistate Variant[a]

	V_{ij} (meV)		
	CT_1	CT_2	CT_3
GS	10.0 (270.0)	0.7 (67.1)	4.4 (4.3)
LE_1	43.6 (43.9)	20.2 (9.6)	14.8 (7.2)
LE_2	4.1 (10.1)	6.1 (11.2)	9.2 (9.7)
LE_3	32.8 (97.8)	24.0 (25.0)	9.4 (16.1)

[a] V_{ij} values estimated under the two-state FCD approximation are included within parentheses for comparison purposes.

https://doi.org/10.1021/acs.jpca.1c05740
J. Phys. Chem. A 2021, 125, 9982−9994

tions.[44,49] Regarding the CS process, the V_{ij} couplings computed for the electron transfer between the local excited states LE_{1-3} to the first CT_1 excited state show, in general, the largest values (43.6, 4.1, and 32.8 meV for $V_{LE1-CT1}$, $V_{LE2-CT1}$, and $V_{LE3-CT1}$, respectively). These V_{ij} values are consistent with the nature of the S_1 state, which is a CT-like state but with a non-negligible mixing of LE excitations as suggested by the value of Δq (1.23) and the attachment/detachment densities (Figure 3b). For the CR process, the couplings between the three lowest CT_{1-3} states and the ground state are calculated to be 10.0, 0.7, and 4.4 meV, respectively (Table 1). Thus, the CR event between CT_1 and GS is the most plausible recombination pathway.

It is interesting to compare the above results with the V_{ij} couplings calculated by employing the two-state FCD variant, which is the most widely used approach in the electron-transfer context.[47,85] However, in complex scenarios where a dense manifold of low-lying excited states close in energy is present, as is the case of truxTTF·$C_{30}H_{12}$ and many other heterojunction systems,[49] the two-state FCD approximation is insufficient to provide an adequate description of the electronic couplings between the states involved in the electron-transfer processes. As can be seen in Table 1, the two-state FCD diabatization scheme yields reasonable V_{ij} couplings for the CS process, with values similar to those obtained with the more accurate multistate FCD variant. An exception is found for the coupling between LE_3 and CT_1, with a significantly larger $V_{LE3-CT1}$ value of 97.8 meV for the two-state FCD approach compared to the multistate variant (32.8 meV). The large $V_{LE3-CT1}$ coupling obtained from the two-state FCD approximation would suggest the electron transfer from the highest-energy local excited state (S_6) to the lowest CT state (S_1) as the most probable CS pathway, which is at odds with the multistate FCD picture. Concerning the CR process, the descriptions provided by two-state and multistate FCD approximations are largely divergent. In particular, the V_{CT1-GS} and V_{CT2-GS} couplings computed with the two-state FCD variant are significantly overestimated (270.0 and 67.1 meV, respectively) compared to the values predicted with the multistate FCD scheme (10.0 and 0.7 meV, respectively). The highly overestimated V_{CT1-GS} and V_{CT2-GS} values obtained within the two-state FCD scheme are clearly artifacts, highlighting the importance of including multistate effects for accurate coupling predictions in the donor−acceptor truxTTF·$C_{30}H_{12}$ heterodimer. The overestimation of the CR couplings by the two-state FCD approach is in line with recent findings reported by Kastinen et al.,[49] who also employed an optimally tuned LC density functional. Our results therefore reveal that the multistate FCD variant is highly recommended in those cases where different electron-transfer pathways (either charge-separation or charge-recombination) can occur as a consequence of the presence of a large number of excited states in a narrow energy window.

Gibbs Free Energy Difference. To estimate the free energy difference for the CS and CR processes (ΔG_{CS} and ΔG_{CR}), the optimization of the lowest-energy charge-transfer (CT_1, CT_2, and CT_3) and local (LE_1, LE_2, and LE_3) excited states is required. Figure 4 displays a schematic diagram with the vertical and adiabatic energies calculated for the three lowest-energy CT and LE excited states of the truxTTF·$C_{30}H_{12}$ heterodimer in *o*-dichlorobenzene within the SS-PCM approach. Table 2 collects all of the ΔG_{CS} and ΔG_{CR} values computed for truxTTF·$C_{30}H_{12}$, which are further employed for

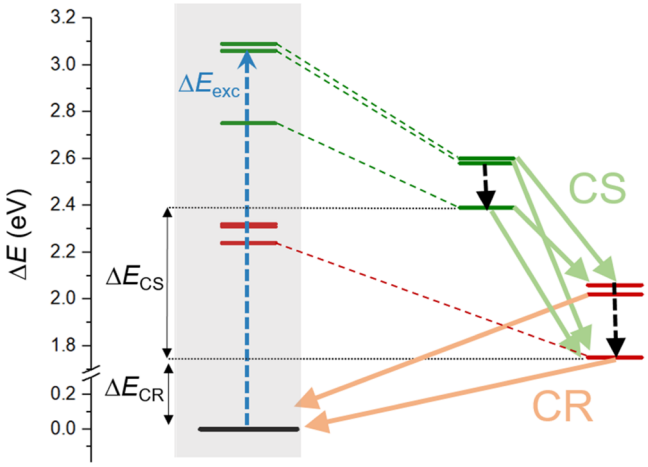

Figure 4. Schematic diagram of the computed excited states of interest indicating the ΔE_{CS} and ΔE_{CR} energy differences. Excitation energies at the Franck−Condon region are included in the gray rectangle. On the right, the excited-state energies at the estimated minimum-energy geometries to compute ΔE_{CS} and ΔE_{CR} are shown. Color code: black is used for the ground state, red for CT states (*i.e.*, $|D^+A^-\rangle$), and green for LE states ($|D^*A\rangle$).

the calculation of the CS and CR rate constants (see below). The Gibbs free energy differences ΔG are approximated by assuming to be similar to the adiabatic energy differences ΔE (*i.e.*, $\Delta G_{CS} \approx \Delta E_{CS}$ and $\Delta G_{CR} \approx \Delta E_{CR}$).[41,44]

Prior to discussing the adiabatic energy differences ΔE_{CS} and ΔE_{CR}, it is interesting to compare the vertical excitation energies (Frank−Condon region) calculated for the lowest-energy excited states of truxTTF·$C_{30}H_{12}$ at the OT-LC-BLYP(ω = 0.16 $bohr^{-1}$)/6-31G** level in *o*-dichlorobenzene within both the linear-response and the state-specific PCM approach. TDA−DFT within the SS-PCM approximation predicts excitation energies of 2.22, 2.29, and 2.35 eV for the GS → CT_1, GS → CT_2, and GS → CT_3 transitions, respectively (Table S11). These transitions are strongly stabilized (by *ca.* 0.4−0.7 eV) when compared to the vertical excitations obtained using the standard linear-response PCM formalism (2.69, 2.88, and 2.95 eV for the GS → CT_1, GS → CT_2, and GS → CT_3 transitions, respectively, Table S8). Note that practically identical excitation energies (2.69, 2.87, and 2.91 eV, respectively) are found when computed in the gas phase. These outcomes highlight the relevance of using the SS-PCM approach, which accounts for the density of the specific state instead of the transition density, to properly capture the expected stabilization of the CT-like excited states by solvent effects (polarization and relaxation). The notorious energy stabilization found for the CT excitations when using the SS-PCM approach is in line with previous studies.[39,86] The polarization and relaxation solvent effects described by SS-PCM are, therefore, necessary for the correct prediction of ΔG_{CS} and ΔG_{CR} and, consequently, for the accurate estimation of the CS and CR electron-transfer rate constants. In contrast to the CT-type transitions, the LE excitation energies, for which solvent effects are expected to be less important, barely show differences between the two PCM approaches (Table S11).

We now turn our attention to the adiabatic energies obtained by full-geometry optimization of the low-lying excited states of interest. The CT_1 state of truxTTF·$C_{30}H_{12}$ was initially optimized at the OT-LC-BLYP(ω = 0.16 $bohr^{-1}$)/6-

https://doi.org/10.1021/acs.jpca.1c05740
J. Phys. Chem. A 2021, 125, 9982−9994

31G** level in the presence of *o*-dichlorobenzene with the linear-response PCM approach. The minimum-energy structure of this CT state displays shorter intermolecular distances compared to the ground-state geometry, in concordance with the enhanced attractive Coulombic interaction between the donor truxTTF and acceptor $C_{30}H_{12}$ units in this state. This structural rearrangement in CT_1 from the ground-state geometry (Franck−Condon region) is accompanied by a relaxation energy of 0.49 eV. The CT_1 energy at the optimized geometry within the linear-response PCM scheme was additionally refined using the equilibrium SS-PCM approach, to take into account the stabilization due to the environmental effects (~0.50 eV). The adiabatic energy difference between CT_1 and GS ($\Delta E_{CT1\text{-}GS} = \Delta E_{CR} \approx \Delta G_{CR}$) was thereby estimated to be 1.75 eV. For the other low-lying CT states (CT_2 and CT_3), it was safely assumed that their minimum-energy geometries were similar to that obtained for the CT_1 state. Consequently, the energy of the CT_2 and CT_3 excited states was recalculated with the equilibrium SS-PCM approach at the CT_1-optimized truxTTF$^+$·$C_{30}H_{12}^-$ geometry. The corresponding adiabatic $\Delta E_{CT2\text{-}GS}$ and $\Delta E_{CT3\text{-}GS}$ energies after solvent corrections were estimated to be 2.02 and 2.08 eV, respectively.

Table 2. Gibbs Free Energy Differences (ΔG) between the Ground State and the CT States and between the LE and CT Excited States Involved in the CR and CS Electronic Processes Computed at the OT-LC-BLYP(ω = 0.16 bohr^{-1})/6−31G Level in *o*-Dichlorobenzene within the SS-PCM Approximation**

	ΔG (eV)		
	CT_1	CT_2	CT_3
GS	−1.75	−2.02	−2.08
LE_1	−0.70	−0.43	−0.37
LE_2	−0.86	−0.59	−0.53
LE_3	−0.87	−0.60	−0.54

The optimization of the local excited states (LE_1, LE_2, and LE_3) of the supramolecular truxTTF·$C_{30}H_{12}$ heterodimer was less feasible. Convergence problems in excited-state optimizations often appear when there is a manifold of excited states of similar nature in a narrow energy window. To circumvent this technical issue, and considering that these excitations are totally centered on the donor truxTTF unit, the energies of the LE_1, LE_2, and LE_3 minima were estimated by correcting the vertical excitation energies ΔE_{exc} at the ground-state geometry of truxTTF·$C_{30}H_{12}$ with the relaxation energies ΔE_{rel} obtained from the optimization of the three first singlet excited states of the isolated truxTTF moiety (0.30, 0.46, and 0.47 eV for LE_1, LE_2, and LE_3, respectively). The estimated adiabatic energy differences for the local excited states ΔE_{LE1-GS}, ΔE_{LE2-GS}, and ΔE_{LE3-GS} were then calculated to be 2.45, 2.61, and 2.62 eV, respectively (Figure 4).

In line with the picture found at the Franck−Condon region, Figure 4 clearly shows that there are two sets of excited states well-separated in energy: the three lowest-energy CT excited states and the LE excitations, LE_1 being an almost dark state and LE_2 and LE_3 being bright states (Table S11). As the energy difference between LE_2/LE_3 and LE_1 local excited states is small (<0.2 eV), an internal conversion from the bright states to the LE_1 state is likely to take place. The CS process can thus occur from this LE_1 state to any CT state (CT_{1-3}). Finally, the CR process is meant to occur from the lowest-energy CT_1 state, after internal conversion, to the ground state. Nonetheless, the CS and CR rate constants for all of the possible charge-transfer pathways were computed as detailed below.

Internal and External Reorganization Energy. The internal reorganization energy λ_{int} of the CS and CR processes (λ_{int}^{CS} and λ_{int}^{CR}) was computed according to eqs S5 and S6, respectively, for which the energies calculated for the isolated truxTTF and $C_{30}H_{12}$ compounds are employed (Figure S5). The energies of the donor and acceptor species were computed using the OT-LC-BLYP density functional with optimized ω values of 0.03 and 0.04 bohr^{-1} for truxTTF and $C_{30}H_{12}$, respectively. For the CS process, the internal reorganization components of the truxTTF and $C_{30}H_{12}$ units were calculated to be 0.50 and 0.06 eV, respectively, being λ_{int}^{CS} = 0.56 eV. For CR, a smaller λ_{int}^{CR} value of 0.13 eV is predicted, with internal reorganization components of 0.07 and 0.06 eV for truxTTF and $C_{30}H_{12}$, respectively. A quick comparison of the λ_{int}^{CS} and λ_{int}^{CR} values reveals that the energy difference between the two magnitudes (0.43 eV) mainly comes from the donor truxTTF unit and is due to the difference between the equilibrium structures obtained for truxTTF in its excited state and in its cation/neutral ground state (Figure S6). In contrast, the internal reorganization energy components for $C_{30}H_{12}$ in both CS and CR processes present a similar and small value (0.06 eV) due to the rigidity of the $C_{30}H_{12}$ buckybowl.

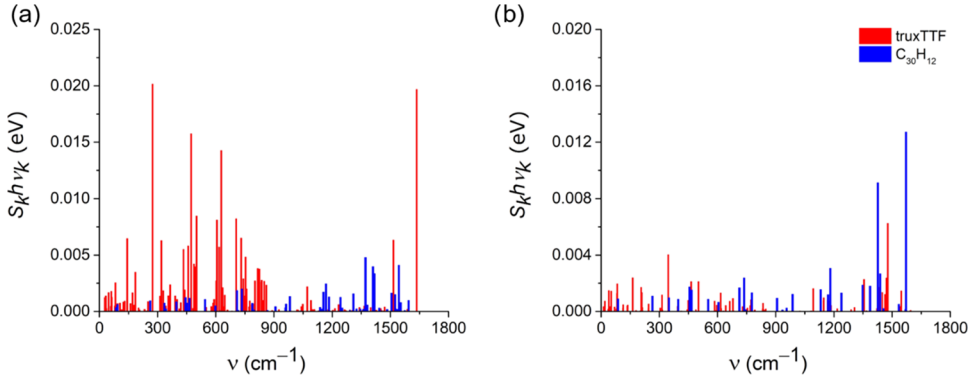

Figure 5. Contribution of each normal mode to the internal reorganization energy of (a) the charge-separation and (b) charge-recombination processes calculated at the OT-LC-BLYP/6-31G** level, with ω values of 0.03 and 0.04 bohr^{-1} for the isolated truxTTF and $C_{30}H_{12}$ compounds, respectively.

https://doi.org/10.1021/acs.jpca.1c05740
J. Phys. Chem. A 2021, 125, 9982−9994

The internal reorganization energies of the CS and CR events have been additionally decomposed in contributions for each vibrational normal mode by calculating the HR factors according to Malagoli et al.[87] (see the Supporting Information for further details). Figure 5 displays the decomposition of λ_{int}^{CS} and λ_{int}^{CR} in the vibrational modes of the isolated truxTTF and $C_{30}H_{12}$ compounds calculated at their respective OT-LC-BLYP/6−31G** level. For CS (Figure 5a), truxTTF possesses many active vibrations along the frequency spectrum. Among them, there are four normal modes calculated at 274, 473, 628, and 1636 cm^{-1} showing especially large contributions to λ_{int}^{CS}. The low-frequency vibrations (below 1000 cm^{-1}) correspond to either the bendings of the truxTTF core or rotations of the dithiole rings (Figure S6a), whereas the high-frequency mode (1636 cm^{-1}) is related to the stretching of single and double carbon−carbon (C−C/C═C) bonds of the π-conjugated truxTTF skeleton. For the $C_{30}H_{12}$ hemifullerene, four high-frequency vibrations computed at 1371, 1410, 1418, and 1544 cm^{-1} and associated with C−C/C═C bond stretchings are responsible for the highest contributions to λ_{int}^{CS}. For CR (Figure 5b), the λ_{int}^{CR} decomposition is much simpler compared to the CS process, presenting only three high-frequency vibrations with significant contributions: one active normal mode for truxTTF (1478 cm^{-1}) and two vibrations for $C_{30}H_{12}$ (1426 and 1571 cm^{-1}). These normal modes are also described by stretchings of C−C/C═C bonds.

All frequencies higher than 250 cm^{-1} were treated quantum mechanically and condensed in an effective vibration. The frequency for this effective vibration was computed as $\nu_{eff} = \sum_{\nu_k>250} S_k\nu_k / \sum_{\nu_k>250} S_k$, giving a ν_{eff} value of 683 cm^{-1} for the CS process. A quantum internal reorganization energy contribution for CS ($\lambda_{int,q}^{CS}$) can be defined as $\lambda_{int,q}^{CS} = \sum_{\nu_k>250} h\nu_k S_k$ with a value of 1816 cm^{-1}. This $\lambda_{int,q}^{CS}$ contribution must be recovered by the reorganization energy inferred from the effective vibration (*i.e.*, $\lambda_{int,q}^{CS} = h\nu_{eff}S_{eff}$). From the latter expression, the effective HR factor S_{eff} can then be evaluated (2.66). The computed $\lambda_{int,q}^{CS}$ value of 0.23 eV represents 41% of the total internal reorganization energy for the CS process discussed above (λ_{int}^{CS} = 0.56 eV). The remaining part of the internal reorganization energy, computed as the difference between λ_{int}^{CS} and $\lambda_{int,q}^{CS}$ ($\lambda_{int,c}^{CS} = \lambda_{int}^{CS} - \lambda_{int,q}^{CS}$ = 0.34 eV), is treated classically and included together with the external reorganization energy in λ_c ($\lambda_c = \lambda_{int,c}^{CS} + \lambda_{ext}^{CS}$) in the final rate expression (eq 1). A similar procedure was adopted for the CR process. An effective frequency of 872 cm^{-1} and a S_{eff} = 0.97 were estimated with a quantum internal reorganization energy $\lambda_{int,q}^{CR}$ of 0.10 eV, which is 77% of the internal reorganization energy for that electron-transfer process (0.13 eV). The classical internal reorganization energy $\lambda_{int,c}^{CR}$ is therefore computed to be very small (0.03 eV).

Regarding the external reorganization energy λ_{ext}, different values are expected for the CS and CR processes (λ_{ext}^{CS} and λ_{ext}^{CR}) since the solvent molecules should reorient their positions in response to the different electronic situations. For CS, the solvent molecules should undergo significant polarization and reorganization due to the charged truxTTF$^+$·$C_{30}H_{12}^-$ complex, whereas the rearrangement of the solvent molecules surrounding the neutral truxTTF·$C_{30}H_{12}$ after CR should be smaller. As mentioned above, λ_{ext} was computed using the "nonequilibrium vs equilibrium solvation" model within the SS-PCM approach (see the Supporting Information for additional details).[39] Briefly, the λ_{ext}^{CS} and λ_{ext}^{CR} components were estimated as the energy difference between the total reorganization energy λ, computed according to eqs S9−S12 for the isolated fragments, and the corresponding internal λ_{int}^{CS} and λ_{int}^{CR} contributions. For CS, the λ_{ext}^{CS} is estimated to be 0.89 eV, with 0.38 and 0.51 eV for the truxTTF and $C_{30}H_{12}$ fragment contributions, respectively. A slightly smaller λ_{ext}^{CR} value of 0.72 eV is found for the CR event, with contributions of 0.28 and 0.44 eV for the truxTTF and $C_{30}H_{12}$ moieties, respectively. Note that the λ_{ext}^{CS} and λ_{ext}^{CR} values are significantly larger than those calculated for the internal reorganization energy, and thus, λ_{ext} has a larger impact on the calculation of CS and CR rate constants, in contrast to what occurs in molecular crystals where λ_{ext} is generally small.[88]

As λ_{ext} is estimated from an energy difference between λ and λ_{int}^{CS} or λ_{int}^{CR} (eq S8) at different geometries, the dependence of λ_{ext} with respect to the molecular structure has also been analyzed. To do so, λ_{ext} at a fixed geometry (ground-state geometry for the neutral fragments) is calculated for both charge-transfer CS and CR events. For CS, the nonequilibrium energy component was calculated using the density obtained from the LE_1 excited state/ground state for truxTTF*/$C_{30}H_{12}$, whereas for the equilibrium energy contribution, the density calculated for the cationic/anionic states of truxTTF$^+$/$C_{30}H_{12}^-$ was used. An external reorganization energy of 0.37 eV (0.44 eV) for truxTTF ($C_{30}H_{12}$) was obtained, providing a total external reorganization energy of 0.81 eV. For CR, the external reorganization energy was now computed using the cation/anion densities as the nonequilibrium components and the ground-state density as the equilibrium component. The resulting λ_{ext} values were found to be 0.32 and 0.44 eV for truxTTF and $C_{30}H_{12}$, respectively, being the total external reorganization energy of 0.76 eV. The similarity between the external reorganization energy values computed at a fixed geometry (0.81 and 0.76 eV for CS and CR, respectively) and the λ_{ext}^{CS} and λ_{ext}^{CR} values calculated above (0.89 and 0.72 eV) indicates that there is a small influence of the internal molecular structure on the solvent reorganization energy.

Charge-Separation (k_{CS}) and Charge-Recombination (k_{CR}) Rates. In the previous sections, all of the parameters needed to estimate the electron-transfer rates using the MLJ equation (eq 1) have been computed and discussed. Table 3 presents all of the relevant parameters and the values computed for the k_{CS} and k_{CR} rate constants of the different electron-transfer pathways in the truxTTF·$C_{30}H_{12}$ heterodimer, whereas Figure 6 shows a schematic picture of the kinetical relevance of the different electron-transfer channels. For CS, the fastest electron-transfer rate constants are found to be those occurring from the initial LE_1 (S_4) and LE_3 (S_6) excited states to the final CT_1 (S_1) state with CS rates of 2.0×10^{12} and 3.0×10^{12} s^{-1}, respectively, which are in good agreement with the reported experimental rate of 6.6×10^{11} s^{-1}.[23] Although our results indicate that the most probable pathway for charge separation is from LE_3 to CT_1, an ultrafast internal conversion from LE_3 to LE_1 together with a slower $LE_1 \rightarrow CT_1$ CS transition would also be feasible. After the CS event, CR takes place from the lowest-energy CT_1 state to the ground state with a CR rate constant k_{CR} of 2.6×10^9 s^{-1}, also in reasonably good accord with the experimentally estimated rate constant (1.0×10^{10} s^{-1}).[23] The constant rates for the most relevant pathways ($LE_1 \rightarrow CT_1$, $LE_3 \rightarrow CT_1$, and $CT_1 \rightarrow$ GS) have also been computed with the Marcus theory for comparison purposes (see the Supporting Information for further details).

https://doi.org/10.1021/acs.jpca.1c05740
J. Phys. Chem. A 2021, 125, 9982−9994

Table 3. Relevant Parameters (V_{ij}, ΔG_{ij}, λ_c, S_{eff}, and ν_{eff}, in eV) and Estimated k_{CS} and k_{CR} Rate Constants (in s^{-1}) for the Different Electron-Transfer Pathways in the Donor-Acceptor truxTTF·$C_{30}H_{12}$ Heterodimer

transition	V_{ij}	$-\Delta G_{ij}$	λ_c	S_{eff}	ν_{eff}[a]	k_{ij}
CS process						
$LE_1 \rightarrow CT_1$	0.044	0.74	1.23	2.66	0.085 (683)	2.0×10^{12}
$LE_1 \rightarrow CT_2$	0.020	0.47	1.23	2.66	0.085 (683)	2.2×10^{10}
$LE_1 \rightarrow CT_3$	0.015	0.41	1.23	2.66	0.085 (683)	4.7×10^{9}
$LE_2 \rightarrow CT_1$	0.004	0.83	1.23	2.66	0.085 (683)	3.8×10^{10}
$LE_2 \rightarrow CT_2$	0.006	0.56	1.23	2.66	0.085 (683)	6.0×10^{9}
$LE_2 \rightarrow CT_3$	0.009	0.50	1.23	2.66	0.085 (683)	6.6×10^{9}
$LE_3 \rightarrow CT_1$	0.033	0.84	1.23	2.66	0.085 (683)	3.0×10^{12}
$LE_3 \rightarrow CT_2$	0.024	0.57	1.23	2.66	0.085 (683)	1.3×10^{11}
$LE_3 \rightarrow CT_3$	0.009	0.51	1.23	2.66	0.085 (683)	1.0×10^{10}
CR process						
$CT_1 \rightarrow GS$	0.010	1.75	0.75	0.97	0.108 (872)	2.6×10^{9}
$CT_2 \rightarrow GS$	0.001	2.02	0.75	0.97	0.108 (872)	1.7×10^{5}
$CT_3 \rightarrow GS$	0.004	2.08	0.75	0.97	0.108 (872)	2.3×10^{4}

[a]Values within parentheses are in cm^{-1}.

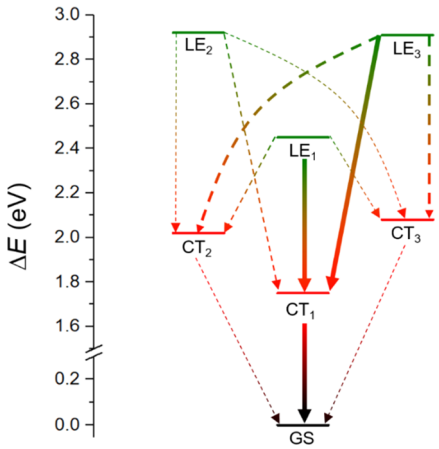

Figure 6. Scheme for all of the CS and CR pathways. The thickness of the arrows indicates the relevance of the decay channels according to Table 3.

Finally, to analyze the effect of the supramolecular organization on the CS and CR rates, the electron-transfer processes were evaluated for the minimum-energy structures **2** and **3** of the truxTTF·$C_{30}H_{12}$ heterodimer displayed in Figure 2. The values computed for the relevant parameters and the rate constants of **2** and **3**, respectively, are presented in Tables S12 and S13. Structure **1** in Figure 2 does not present favorable charge-transfer processes as discussed below. The highest k_{CS}/k_{CR} rates for structures **2** and **3** are calculated to be 1.4×10^{11}/4.3×10^{9} and 8.6×10^{10}/1.7×10^{8} s^{-1}, respectively. The fastest CS events are, therefore, found for structure **4** (2.0 and 3.0×10^{12} s^{-1}), which exhibits electronic states with high electronic couplings and ΔG_{CS} values near the resonance with respect to the reorganization energy (see Table 3 and Tables S12 and S13). A closer analysis of the adiabatic excitation energies for all of the structures (Table S14) highlights that those supramolecular arrangements with C···S intermolecular interactions, irrespective of the staggered or bowl-in-bowl organization (*i.e.*, structures **2** and **4**), tend to stabilize a larger number of CT-type excited states below the lowest-energy LE excited states, thus opening the door for different and efficient charge-separation pathways. Structure **3**, which is a staggered arrangement with no C···S interactions, presents only one accessible CT excited state below the LE states for a favorable CS event. Surprisingly, structure **1** with a bowl-in-bowl disposition and optimal π-π interactions made only by C···C intermolecular contacts does not present CT excited states below the lowest-energy LE states and, consequently, no photoinduced electron-transfer is expected for this supramolecular structure. Finally, the CR process takes place in the inverted Marcus regime with similar k_{CR} rate constants around $(3-4) \times 10^{9}$ s^{-1} for structures **2** and **4** and one order of magnitude slower for structure **3**.

Charge-Separation and Charge-Recombination Kinetic Model. To obtain a global picture of the CS and CR electronic events for structures **2**, **3**, and **4**, a simple kinetic model including all of the previously computed rate constants for the different decay pathways was built (see the Supporting Information for further details). Figure 7 displays a global representation of the time evolution of the populations of the electronic states according to their nature (LE, CT, and GS) calculated for structures **2**, **3**, and **4**, whereas Figure S8 shows the populations for each particular excited state as a function of time. A detailed inspection of Figure 7 reveals that the fastest CS electron-transfer process occurs for structure **4**. Actually, a decrease of 50% (99%) in population for LE states is achieved after 18.8 (215), 50.0 (416), and 0.5 (2.9) ps for structures **2**, **3**, and **4**, respectively. Nevertheless, it should be noted that the nonradiative CS mechanism for structures **2**, **3**, and **4** is different (Figure S8). For structures **2** and **3**, the CS deactivation pathway occurs from the LE_1 state after a faster downhill internal conversion from the bright states (LE_2 and LE_3 states). On the contrary, a direct charge separation takes place from the bright states (LE_2 and LE_3) for structure **4** because the $LE_3 \rightarrow CT_1$ charge separation rate is competitive with the nonradiative $LE_3 \rightarrow LE_1$ internal conversion. For CR, an increase in the population of 50% for the ground state is calculated to occur at 0.24, 4.16, and 0.32 ns for structures **2**, **3**, and **4**, respectively. Interestingly, the half-life times estimated from populations of the LE, CT, and GS states are used to compute global effective rates for the CS and CR processes in a more intuitive and simplified three-state picture. Our kinetic model leads to global CS (CR) rate constants of 5.3×10^{10}, 2.0×10^{10}, and 2.0×10^{12} s^{-1} (4.3×10^{9}, 2.4×10^{8}, 3.1×10^{9} s^{-1}) for structures **2**, **3**, and **4**, respectively. Note that the theoretical global rates calculated for structure **4** (the most stable) are in good accord with the global experimental values estimated from spectroscopic measurements (6.6×10^{11} and 1.0×10^{10} s^{-1} for CS and CR events, respectively).

CONCLUSIONS

In this work, we have proposed a theoretical protocol to accurately predict charge-separation (CS) and charge-recombination (CR) rate constants for a donor−acceptor (D−A) buckybowl-based supramolecular complex (truxTTF·$C_{30}H_{12}$). The computational approach combines the Marcus−Levich−

https://doi.org/10.1021/acs.jpca.1c05740
J. Phys. Chem. A 2021, 125, 9982−9994

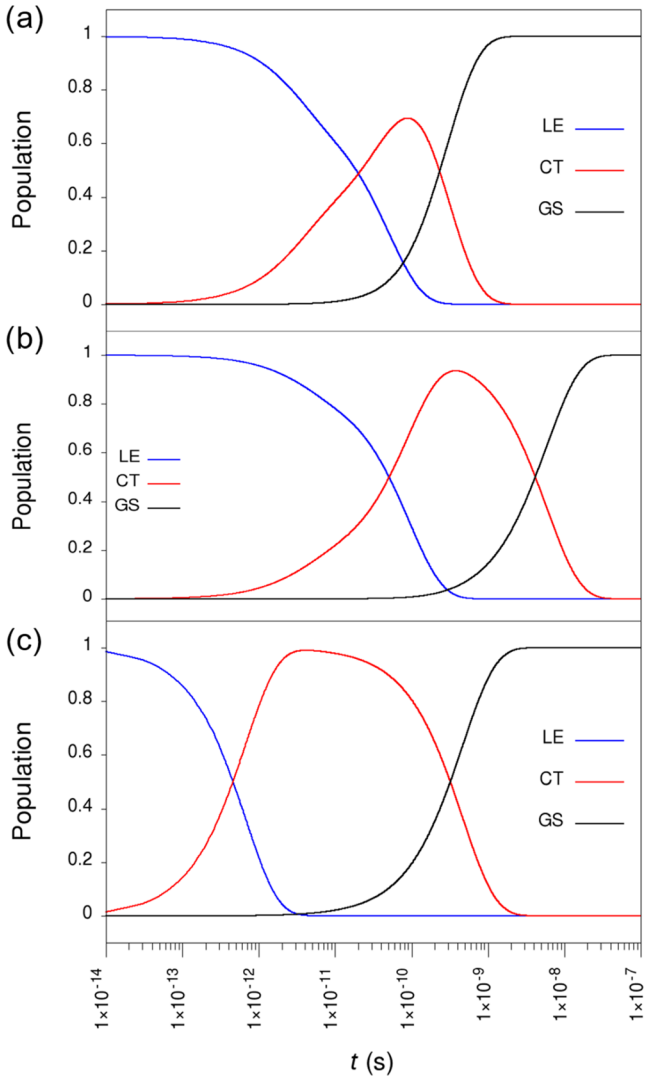

Figure 7. Time evolution of the populations of the electronic states according to their nature (LE, CT, and GS) calculated for structures **2** (a), **3** (b), and **4** (c) according to the kinetic model proposed (see the Supporting Information for further details). Time (*x*-axis) is represented in the logarithmic scale.

Jortner (MLJ) rate expression together with electronic structure calculations (at the DFT and TDDFT level) and a multistate diabatization method (an extended fragment charge difference scheme[58]) to carefully calculate the different terms entering into the rate expression (*i.e.*, electronic couplings, reorganization energy, and Gibbs free energy difference). Our results clearly disclose that optimally tuned (OT) long-range corrected (LC) density functionals are necessary to provide a correct energy ordering of the low-lying excited states. The OT-LC-BLYP predicts a complex scenario with at least six, low-lying, close-in-energy excited states of local and CT character potentially involved in the CS and CR processes. In this context, which can be generally found in many other D−A heterojunctions, the inclusion of multistate effects is shown to have a strong impact on the accurate estimation of the electronic couplings. We also demonstrate the relevance of the correct stabilization of the CT states due to the solvent effect, accounted using the state-specific PCM solvation model. After the careful estimation of all of the specific CS and CR rate constants for the different deactivation pathways, a simple but insightful kinetic model is proposed to estimate the global CS and CR rate constants in an effective three-state picture. The values computed for the global CS and CR rates of the donor−acceptor truxTTF·$C_{30}H_{12}$ supramolecular complex are found to be in good agreement with the experimental values. The suggested theoretical protocol including multistate effects and an accurate state-specific description of the solvent effects is of general application to any other D−A molecular or supramolecular system with potential for organic solar cells.

■ ASSOCIATED CONTENT

Supporting Information

The Supporting Information is available free of charge at https://pubs.acs.org/doi/10.1021/acs.jpca.1c05740.

Additional theoretical details, excited-state analysis, estimation of reorganization energies, excitations and electronic couplings for structures **1**, **2**, and **3**, and details about the kinetic model (PDF)

■ AUTHOR INFORMATION

Corresponding Author

Juan Aragó − *Instituto de Ciencia Molecular (ICMol), Universidad de Valencia, Paterna 46980, Spain;* orcid.org/0000-0002-0415-9946; Email: juan.arago@uv.es

Authors

Jesús Cerdá − *Instituto de Ciencia Molecular (ICMol), Universidad de Valencia, Paterna 46980, Spain;* orcid.org/0000-0002-5008-376X

Joaquín Calbo − *Instituto de Ciencia Molecular (ICMol), Universidad de Valencia, Paterna 46980, Spain;* orcid.org/0000-0003-4729-0757

Enrique Ortí − *Instituto de Ciencia Molecular (ICMol), Universidad de Valencia, Paterna 46980, Spain;* orcid.org/0000-0001-9544-8286

Complete contact information is available at: https://pubs.acs.org/10.1021/acs.jpca.1c05740

Author Contributions

The manuscript was written through contributions of all authors. All authors have given approval to the final version of the manuscript.

Notes

The authors declare no competing financial interest.

■ ACKNOWLEDGMENTS

This work was supported by the Spanish Ministry of Science and Innovation (MICINN) (projects PGC2018-099568-B-I00, RED2018-102815-T, and RED2018-102331-T), the Generalitat Valenciana (PROMETEO/2020/077 and SEJI/2018/035), and European Feder funds (PGC2018-099568-B-I00). J.A. and J. Cerdá are grateful to the MICINN for their "Ramon-y-Cajal" (RyC-2017-23500) and predoctoral (BES-2016-076826) grants, respectively.

■ REFERENCES

(1) Yu, G.; Gao, J.; Hummelen, J. C.; Wudl, F.; Heeger, A. J. Polymer Photovoltaic Cells: Enhanced Efficiencies via a Network of Internal Donor-Acceptor Heterojunctions. *Science* **1995**, *270*, 1789−1791.

(2) Halls, J. J. M.; Walsh, C. A.; Greenham, N. C.; Marseglia, E. A.; Friend, R. H.; Moratti, S. C.; Holmes, A. B. Efficient Photodiodes from Interpenetrating Polymer Networks. *Nature* **1995**, *376*, 498−500.
(3) Thompson, B. C.; Fréchet, J. M. J. Polymer−Fullerene Composite Solar Cells. *Angew. Chem., Int. Ed.* **2008**, *47*, 58−77.
(4) Meng, L.; Zhang, Y.; Wan, X.; Li, C.; Zhang, X.; Wang, Y.; Ke, X.; Xiao, Z.; Ding, L.; Xia, R.; Yip, H. L.; Cao, Y.; Chen, Y. Organic and Solution-Processed Tandem Solar Cells with 17.3% Efficiency. *Science* **2018**, *361*, 1094−1098.
(5) Liu, Q.; Jiang, Y.; Jin, K.; Qin, J.; Xu, J.; Li, W.; Xiong, J.; Liu, J.; Xiao, Z.; Sun, K.; Yang, S.; Zhang, X.; Ding, L. 18% Efficiency Organic Solar Cells. *Sci. Bull.* **2020**, *65*, 272−275.
(6) Günes, S.; Neugebauer, H.; Sariciftci, N. S. Conjugated Polymer-Based Organic Solar Cells. *Chem. Rev.* **2007**, *107*, 1324−1338.
(7) Jariwala, D.; Sangwan, V. K.; Lauhon, L. J.; Marks, T. J.; Hersam, M. C. Carbon Nanomaterials for Electronics, Optoelectronics, Photovoltaics, and Sensing. *Chem. Soc. Rev.* **2013**, *42*, 2824−2860.
(8) Saunders, B. R.; Turner, M. L. Nanoparticle−Polymer Photovoltaic Cells. *Adv. Colloid Interface Sci.* **2008**, *138*, 1−23.
(9) Delgado, J. L.; Bouit, P.-A.; Filippone, S.; Herranz, M. A.; Martín, N. Organic Photovoltaics: A Chemical Approachw. *Chem. Commun.* **2010**, *46*, 4853−4865.
(10) Kennedy, R. D.; Ayzner, A. L.; Wanger, D. D.; Day, C. T.; Halim, M.; Khan, S. I.; Tolbert, S. H.; Schwartz, B. J.; Rubin, Y. Self-Assembling Fullerenes for Improved Bulk-Heterojunction Photovoltaic Devices. *J. Am. Chem. Soc.* **2008**, *130*, 17290−17292.
(11) Deibel, C.; Dyakonov, V. Polymer−Fullerene Bulk Heterojunction Solar Cells. *Rep. Prog. Phys.* **2010**, *73*, No. 096401.
(12) Deibel, C.; Dyakonov, V.; Brabec, C. J. Organic Bulk-Heterojunction Solar Cells. *IEEE J. Sel. Top. Quantum Electron.* **2010**, *16*, 1517−1527.
(13) Li, G.; Shrotriya, V.; Huang, J.; Yao, Y.; Moriarty, T.; Emery, K.; Yang, Y. High-Efficiency Solution Processable Polymer Photovoltaic Cells by Self-Organization of Polymer Blends. *Nat. Mater.* **2005**, *4*, 864−868.
(14) Ohkita, H.; Cook, S.; Astuti, Y.; Duffy, W.; Tierney, S.; Zhang, W.; Heeney, M.; McCulloch, I.; Nelson, J.; Bradley, D. D. C.; Durrant, J. R. Charge Carrier Formation in Polythiophene/Fullerene Blend Films Studied by Transient Absorption Spectroscopy. *J. Am. Chem. Soc.* **2008**, *130*, 3030−3042.
(15) Groves, C.; Reid, O. G.; Ginger, D. S. Heterogeneity in Polymer Solar Cells: Local Morphology and Performance in Organic Photovoltaics Studied with Scanning Probe Microscopy. *Acc. Chem. Res.* **2010**, *43*, 612−620.
(16) Suman; Singh, S. P. Impact of End Groups on the Performance of Non-Fullerene Acceptors for Organic Solar Cell Applications. *J. Mater. Chem. A* **2019**, *7*, 22701−22729.
(17) Xian, K.; Cui, Y.; Xu, Y.; Zhang, T.; Hong, L.; Yao, H.; An, C.; Hou, J. Efficient Exciton Dissociation Enabled by the End Group Modification in Non-Fullerene Acceptors. *J. Phys. Chem. C* **2020**, *124*, 7691−7698.
(18) Privado, M.; Malhotra, P.; de la Cruz, P.; Singhal, R.; Cerdá, J.; Aragó, J.; Ortí, E.; Sharma, G. D.; Langa, F. Ternary Organic Solar Cell with a Near-Infrared Absorbing Selenophene−Diketopyrrolopyrrole-Based Nonfullerene Acceptor and an Efficiency above 10%. *Sol. RRL* **2020**, *4*, No. 1900471.
(19) Hou, J.; Inganas, O.; Friend, R. H.; Gao, F. Organic Solar Cells Based on Non-Fullerene Acceptors. *Nat. Mater.* **2018**, *17*, 119−128.
(20) Hagen, S.; Bratcher, M. S.; Erickson, M. S.; Zimmermann, G.; Scott, L. T. Novel Syntheses of Three C30H12 Bowl-Shaped Polycyclic Aromatic Hydrocarbons. *Angew. Chem., Int. Ed.* **1997**, *36*, 406−408.
(21) Chen, M.-K.; Hsin, H.-J.; Wu, T.-C.; Kang, B.-Y.; Lee, Y.-W.; Kuo, M.-Y.; Wu, Y.-T. Highly Curved Bowl-Shaped Fragments of Fullerenes: Synthesis, Structural Analysis, and Physical Properties. *Chem. − Eur. J.* **2014**, *20*, 598−608.
(22) Wu, T.-C.; Hsin, H.-J.; Kuo, M.-Y.; Li, C.-H.; Wu, Y.-T. Synthesis and Structural Analysis of a Highly Curved Buckybowl Containing Corannulene and Sumanene Fragments. *J. Am. Chem. Soc.* **2011**, *133*, 16319−16321.
(23) Gallego, M.; Calbo, J.; Aragó, J.; Krick Calderon, R. M.; Liquido, F. H.; Iwamoto, T.; Greene, A. K.; Jackson, E. A.; Pérez, E. M.; Ortí, E.; Guldi, D. M.; Scott, L. T.; Martín, N. Electron Transfer in a Supramolecular Associate of a Fullerene Fragment. *Angew. Chem., Int. Ed.* **2014**, *53*, 2170−2175.
(24) Gallego, M.; Calbo, J.; Krick Calderon, R. M.; Pla, P.; Hsieh, Y.-C.; Pérez, E. M.; Wu, Y.-T.; Ortí, E.; Guldi, D. M.; Martín, N. Complexation and Electronic Communication between Corannulene-Based Buckybowls and a Curved Truxene-TTF Donor. *Chem. − Eur. J.* **2017**, *23*, 3666−3673.
(25) Heller, E. R.; Richardson, J. O. Semiclassical Instanton Formulation of Marcus-Levich-Jortner Theory. *J. Chem. Phys.* **2020**, *152*, No. 244117.
(26) Stehr, V.; Fink, R. F.; Tafipolski, M.; Deibel, C.; Engels, B. Comparison of Different Rate Constant Expressions for the Prediction of Charge and Energy Transport in Oligoacenes. *Wiley Interdiscip. Rev.: Comput. Mol. Sci.* **2016**, *6*, 694−720.
(27) Vydrov, O. A.; Scuseria, G. E. Assessment of a Long-Range Corrected Hybrid Functional. *J. Chem. Phys.* **2006**, *125*, No. 234109.
(28) Gräfenstein, J.; Cremer, D. The Self-Interaction Error and the Description of Non-Dynamic Electron Correlation in Density Functional Theory. *Theor. Chem. Acc.* **2009**, *123*, 171−182.
(29) Lundberg, M.; Siegbahn, P. E. M. Quantifying the Effects of the Self-Interaction Error in DFT: When Do the Delocalized States Appear? *J. Chem. Phys.* **2005**, *122*, No. 224103.
(30) Yanai, T.; Tew, D. P.; Handy, N. C. A New Hybrid Exchange-Correlation Functional Using the Coulomb-Attenuating Method (CAM-B3LYP). *Chem. Phys. Lett.* **2004**, *393*, 51−57.
(31) Chai, J. Da.; Head-Gordon, M. Systematic Optimization of Long-Range Corrected Hybrid Density Functionals. *J. Chem. Phys.* **2008**, *128*, No. 084106.
(32) Adamo, C.; Jacquemin, D. The Calculations of Excited-State Properties with Time-Dependent Density Functional Theory. *Chem. Soc. Rev.* **2013**, *42*, 845−856.
(33) Yi, Y.; Coropceanu, V.; Brédas, J. L. Exciton-Dissociation and Charge-Recombination Processes in Pentacene/C 60 Solar Cells: Theoretical Insight into the Impact of Interface Geometry. *J. Am. Chem. Soc.* **2009**, *131*, 15777−15783.
(34) Zhang, C. R.; Sears, J. S.; Yang, B.; Aziz, S. G.; Coropceanu, V.; Brédas, J. L. Theoretical Study of the Local and Charge-Transfer Excitations in Model Complexes of Pentacene-C60 Using Tuned Range-Separated Hybrid Functionals. *J. Chem. Theory Comput.* **2014**, *10*, 2379−2388.
(35) Yang, B.; Yi, Y.; Zhang, C. R.; Aziz, S. G.; Coropceanu, V.; Brédas, J. L. Impact of Electron Delocalization on the Nature of the Charge-Transfer States in Model Pentacene/C60 Interfaces: A Density Functional Theory Study. *J. Phys. Chem. C* **2014**, *118*, 27648−27656.
(36) Stein, T.; Kronik, L.; Baer, R. Reliable Prediction of Charge Transfer Excitations in Molecular Complexes Using Time-Dependent Density Functional Theory. *J. Am. Chem. Soc.* **2009**, *131*, 2818−2820.
(37) Körzdörfer, T.; Brédas, J.-L. Organic Electronic Materials: Recent Advances in the DFT Description of the Ground and Excited States Using Tuned Range-Separated Hybrid Functionals. *Acc. Chem. Res.* **2014**, *47*, 3284−3291.
(38) Scalmani, G.; Frisch, M. J. Continuous Surface Charge Polarizable Continuum Models of Solvation. I. General Formalism. *J. Chem. Phys.* **2010**, *132*, No. 114110.
(39) Improta, R.; Barone, V.; Scalmani, G.; Frisch, M. J. A State-Specific Polarizable Continuum Model Time Dependent Density Functional Theory Method for Excited State Calculations in Solution. *J. Chem. Phys.* **2006**, *125*, No. 054103.
(40) Su, Y.; Ren, H.; Li, X. Novel Nonequilibrium Solvation Theory for Calculating the Solvatochromic Stokes Shift by State-Specific TD-DFT. *Chem. Phys. Lett.* **2019**, *732*, No. 136640.
(41) Martínez, J. P.; Solà, M.; Voityuk, A. A. Theoretical Estimation of the Rate of Photoinduced Charge Transfer Reactions in

https://doi.org/10.1021/acs.jpca.1c05740
J. Phys. Chem. A 2021, 125, 9982−9994

Triphenylamine C 60 Donor-Acceptor Conjugate. *J. Comput. Chem.* **2016**, *37*, 1396−1405.
(42) Han, J.; Zhang, P.; Aksu, H.; Maiti, B.; Sun, X.; Geva, E.; Dunietz, B. D.; Cheung, M. S. On the Interplay between Electronic Structure and Polarizable Force Fields When Calculating Solution-Phase Charge-Transfer Rates. *J. Chem. Theory Comput.* **2020**, *16*, 6481−6490.
(43) Hsu, C.-P. The Electronic Couplings in Electron Transfer and Excitation Energy Transfer. *Acc. Chem. Res.* **2009**, *42*, 509−518.
(44) Liu, T.; Troisi, A. Absolute Rate of Charge Separation and Recombination in a Molecular Model of the P3HT/PCBM Interface. *J. Phys. Chem. C* **2011**, *115*, 2406−2415.
(45) D'Avino, G.; Olivier, Y.; Muccioli, L.; Beljonne, D. Do Charges Delocalize over Multiple Molecules in Fullerene Derivatives? *J. Mater. Chem. C* **2016**, *4*, 3747−3756.
(46) Cave, R. J.; Newton, M. D. Generalization of the Mulliken-Hush Treatment for the Calculation of Electron Transfer Matrix Elements. *Chem. Phys. Lett.* **1996**, *249*, 15−19.
(47) Voityuk, A. A.; Rösch, N. Fragment Charge Difference Method for Estimating Donor−Acceptor Electronic Coupling: Application to DNA π-Stacks. *J. Chem. Phys.* **2002**, *117*, 5607−5616.
(48) Rust, M.; Lappe, J.; Cave, R. J. Multistate Effects in Calculations of the Electronic Coupling Element for Electron Transfer Using the Generalized Mulliken−Hush Method. *J. Phys. Chem. A* **2002**, *106*, 3930−3940.
(49) Kastinen, T.; Da Silva Filho, D. A.; Paunonen, L.; Linares, M.; Ribeiro Junior, L. A.; Cramariuc, O.; Hukka, T. I. Electronic Couplings and Rates of Excited State Charge Transfer Processes at Poly(Thiophene-: Co -Quinoxaline)-PC71BM Interfaces: Two- versus Multi-State Treatments. *Phys. Chem. Chem. Phys.* **2019**, *21*, 25606−25625.
(50) Jortner, J. Temperature Dependent Activation Energy for Electron Transfer between Biological Molecules. *J. Chem. Phys.* **1976**, *64*, 4860−4867.
(51) Bixon, M.; Jortner, J. *Advances in Chemical Physics*; John Wiley & Sons, Inc., 1999; Vol. *106*, pp 35−202.
(52) Barbara, P. F.; Meyer, T. J.; Ratner, M. A. Contemporary Issues in Electron Transfer Research. *J. Chem. Phys.* **1996**, *100*, 13148−13168.
(53) Troisi, A. Charge Transport in High Mobility Molecular Semiconductors: Classical Models and New Theories. *Chem. Soc. Rev.* **2011**, *40*, 2347−2358.
(54) Fornari, R. P.; Aragó, J.; Troisi, A. A Very General Rate Expression for Charge Hopping in Semiconducting Polymers. *J. Chem. Phys.* **2015**, *142*, No. 184105.
(55) May, V.; Khün, O. *Charge and Energy Transfer Dynamics in Molecular Systems*, 3rd ed.; WILEY-VCH Verlag: Weinheim, Germany, 2011.
(56) Taylor, N. B.; Kassal, I. Generalised Marcus Theory for Multi-Molecular Delocalised Charge Transfer. *Chem. Sci.* **2018**, *9*, 2942−2951.
(57) Mead, C. A.; Truhlar, D. G. Conditions for the Definition of a Strictly Diabatic Electronic Basis for Molecular Systems. *J. Chem. Phys.* **1982**, *77*, 6090−6098.
(58) Yang, C.-H.; Hsu, C.-P. A Multi-State Fragment Charge Difference Approach for Diabatic States in Electron Transfer: Extension and Automation. *J. Chem. Phys.* **2013**, *139*, No. 154104.
(59) Liedtke, M.; Sperlich, A.; Kraus, H.; Baumann, A.; Deibel, C.; Wirix, M. J. M.; Loos, J.; Cardona, C. M.; Dyakonov, V. Triplet Exciton Generation in Bulk-Heterojunction Solar Cells Based on Endohedral Fullerenes. *J. Am. Chem. Soc.* **2011**, *133*, 9088−9094.
(60) Kraus, H.; Heiber, M. C.; Väth, S.; Kern, J.; Deibel, C.; Sperlich, A.; Dyakonov, V. Analysis of Triplet Exciton Loss Pathways in PTB7:PC 71 BM Bulk Heterojunction Solar Cells. *Sci. Rep.* **2016**, *6*, No. 29158.
(61) Chen, T.; Zheng, L.; Yuan, J.; An, Z.; Chen, R.; Tao, Y.; Li, H.; Xie, X.; Huang, W. Understanding the Control of Singlet-Triplet Splitting for Organic Exciton Manipulating: A Combined Theoretical and Experimental Approach. *Sci. Rep.* **2015**, *5*, No. 10923.
(62) Tedlla, B. Z.; Zhu, F.; Cox, M.; Drijkoningen, J.; Manca, J.; Koopmans, B.; Goovaerts, E. Understanding Triplet Formation Pathways in Bulk Heterojunction Polymer:Fullerene Photovoltaic Devices. *Adv. Energy Mater.* **2015**, *5*, No. 1401109.
(63) Tsuneda, T.; Hirao, K. Long-Range Correction for Density Functional Theory. *Wiley Interdiscip. Rev. Comput. Mol. Sci.* **2014**, *4*, 375−390.
(64) Likura, H.; Tsuneda, T.; Yanai, T.; Hirao, K. A Long-Range Correction Scheme for Generalized-Gradient-Approximation Exchange Functionals. *J. Chem. Phys.* **2001**, *115*, 3540−3544.
(65) Körzdörfer, T.; Parrish, R. M.; Marom, N.; Sears, J. S.; Sherrill, C. D.; Brédas, J. L. Assessment of the Performance of Tuned Range-Separated Hybrid Density Functionals in Predicting Accurate Quasiparticle Spectra. *Phys. Rev. B* **2012**, *86*, No. 205110.
(66) Baer, R.; Livshits, E.; Salzner, U. Tuned Range-Separated Hybrids in Density Functional Theory. *Annu. Rev. Phys. Chem.* **2010**, *61*, 85−109.
(67) Karolewski, A.; Kronik, L.; Kümmel, S. Using Optimally Tuned Range Separated Hybrid Functionals in Ground-State Calculations: Consequences and Caveats. *J. Chem. Phys.* **2013**, *138*, No. 204115.
(68) Coropceanu, V.; Cornil, J.; da Silva Filho, D. A.; Olivier, Y.; Silbey, R.; Brédas, J. L. Charge Transport in Organic Semiconductors. *Chem. Rev.* **2007**, *107*, 926−952.
(69) Malagoli, M.; Coropceanu, V.; da Silva Filho, D. A.; Brédas, J. L. A Multimode Analysis of the Gas-Phase Photoelectron Spectra in Oligoacenes. *J. Chem. Phys.* **2004**, *120*, 7490−7496.
(70) Geng, Y.; Wang, J.; Wu, S.; Li, H.; Yu, F.; Yang, G.; Gao, H.; Su, Z. Theoretical Discussions on Electron Transport Properties of Perylene Bisimide Derivatives with Different Molecular Packings and Intermolecular Interactions. *J. Mater. Chem.* **2011**, *21*, 134−143.
(71) Di Donato, E.; Fornari, R. P.; Di Motta, S.; Li, Y.; Wang, Z.; Negri, F. N-Type Charge Transport and Mobility of Fluorinated Perylene Bisimide Semiconductors. *J. Phys. Chem. B* **2010**, *114*, 5327−5334.
(72) Burquel, A.; Lemaur, V.; Beljonne, D.; Lazzaroni, R.; Cornil, J. Pathways for Photoinduced Charge Separation and Recombination at Donor-Acceptor Heterojunctions: The Case of Oligophenylenevinylene-Perylene Bisimide Complexes. *J. Phys. Chem. A* **2006**, *110*, 3447−3453.
(73) Marcus, R. A. On the Theory of Oxidation-Reduction Reactions Involving Electron Transfer. I. *J. Chem. Phys.* **1956**, *24*, 966−978.
(74) Tomasi, J.; And, B. M.; Cammi, R. Quantum Mechanical Continuum Solvation Models. *Chem. Rev.* **2005**, *105*, 2999−3093.
(75) Xu, T.; Yin, S. Effective Polarization Energy of the Naphthalene Molecular Crystal: A Study on the Polarizable Force Field. *Sci. China Chem.* **2014**, *57*, 1375−1382.
(76) Ferrer, F. J.; Improta, R.; Santoro, F.; Barone, V. Computing the Inhomogeneous Broadening of Electronic Transitions in Solution: A First-Principle Quantum Mechanical Approach. *Phys. Chem. Chem. Phys.* **2011**, *13*, 17007−17012.
(77) Frisch, M. J.; Trucks, G. W.; Schlegel, H. B.; Scuseria, G. E.; Robb, M. A.; Cheeseman, J. R.; Scalmani, G.; Barone, V.; Petersson, G. A.; Nakatsuji, H.; Li, X.; Caricato, M.; Marenich, A. V.; Bloino, J.; Janesko, B. G.; Gomperts, R.; Mennucci, B.; Hratchian, H. P.; Ortiz, J. V.; Izmalov, A. F.; Sonnenberg, J. L.; Williams-Young, D.; Ding, F.; Lipparini, F.; Egidi, F.; Goings, J.; Peng, B.; Petrone, A.; Henderson, T.; Ranasinghe, D.; Zakrzewski, V. G.; Gao, J.; Rega, N.; Zheng, G.; Liang, W.; Hada, M.; Ehara, M.; Toyota, K.; Fukuda, R.; Hasegawa, J.; Ishida, M.; Nakajima, T.; Honda, Y.; Kitao, O.; Nakai, H.; Vreven, T.; Throsell, K.; Montgomery, J. A., Jr.; Peralta, J. E.; Ogliaro, F.; Beapark, M. J.; Heyd, J. J.; Brothers, E. N.; Kudin, K. N.; Staroverov, V. N.; Keith, T. A.; Kobayash, R.; Normand, J.; Raghavachari, K.; Rendell, A. P.; Burant, J. C.; Iyengar, S. S.; Tomasi, J.; Cossi, M.; Millam, J. M.; Klene, M.; Adamo, C.; Cammi, R.; Ochterski, J. W.; Martin, R. L.; Morokuma, K.; Farkas, O.; Foresman, J. B.; Fox, D. J. *Gaussian16*; Gaussian Inc.: Wallingford, CT, 2016.

https://doi.org/10.1021/acs.jpca.1c05740
J. Phys. Chem. A 2021, 125, 9982−9994

(78) Hirata, S.; Head-Gordon, M. Time-Dependent Density Functional Theory within the Tamm−Dancoff Approximation. *Chem. Phys. Lett.* **1999**, *314*, 291−299.
(79) Francl, M. M.; Pietro, W. J.; Hehre, W. J.; Binkley, J. S.; Gordon, M. S.; DeFrees, D. J.; Pople, J. A. Self-consistent Molecular Orbital Methods. XXIII. A Polarization-type Basis Set for Second-row Elements. *J. Chem. Phys.* **1982**, *77*, 3654−3665.
(80) Becke, A. D. Density-Functional Exchange-Energy Approximation with Correct Asymptotic Behavior. *Phys. Rev. A* **1988**, *38*, 3098−3100.
(81) Lee, C.; Yang, W.; Parr, R. G. Development of the Colle-Salvetti Correlation-Energy Formula into a Functional of the Electron Density. *Phys. Rev. B* **1988**, *37*, 785−789.
(82) Chai, J. Da.; Head-Gordon, M. Long-Range Corrected Hybrid Density Functionals with Damped Atom-Atom Dispersion Corrections. *Phys. Chem. Chem. Phys.* **2008**, *10*, 6615−6620.
(83) Tomasi, J.; Persico, M. Molecular Interactions in Solution: An Overview of Methods Based on Continuous Distributions of the Solvent. *Chem. Rev.* **1994**, *94*, 2027−2094.
(84) Voityuk, A. A. Electronic Couplings for Photoinduced Electron Transfer and Excitation Energy Transfer Computed Using Excited States of Noninteracting Molecules. *J. Phys. Chem. A* **2017**, *121*, 5414−5419.
(85) Voityuk, A. A. Estimation of Electronic Coupling for Photoinduced Charge Separation and Charge Recombination Using the Fragment Charge Difference Method. *J. Phys. Chem. C* **2013**, *117*, 2670−2675.
(86) Guido, C. A.; Jacquemin, D.; Adamo, C.; Mennucci, B. Electronic Excitations in Solution: The Interplay between State Specific Approaches and a Time-Dependent Density Functional Theory Description. *J. Chem. Theory Comput.* **2015**, *11*, 5782−5790.
(87) Coropceanu, V.; Malagoli, M.; da Silva Filho, D. A.; Gruhn, N. E.; Bill, T. G.; Brédas, J. L. Hole- and Electron-Vibrational Couplings in Oligoacene Crystals: Intramolecular Contributions. *Phys. Rev. Lett.* **2002**, *89*, No. 275503.
(88) Mcmahon, D. P.; Troisi, A. Evaluation of the External Reorganization Energy of Polyacenes. *J. Phys. Chem. Lett.* **2010**, *1*, 941−946.

https://doi.org/10.1021/acs.jpca.1c05740
J. Phys. Chem. A 2021, 125, 9982−9994